Exogenous Superoxide Dismutase Mimetic Without Scavenging H_2O_2 Causes Photoreceptor Damage in a Rat Model for Oxygen-Induced Retinopathy

Shamin Jivabhai Patel,[1] Fayez Bany-Mohammed,[1] Lois McNally,[2,3] Gloria B. Valencia,[4] Douglas R. Lazzaro,[2,3] Jacob V. Aranda,[2–4] and Kay D. Beharry[2–4]

[1]Department of Pediatrics, Division of Neonatal-Perinatal Medicine, University of California-Irvine, Irvine, California, United States
[2]Department of Ophthalmology, State University of New York, Downstate Medical Center, New York, New York, United States
[3]State University of New York Eye Institute, New York, New York, United States
[4]Department of Pediatrics, State University of New York, Downstate Medical Center, New York, New York, United States

Correspondence: Kay D. Beharry, Department of Pediatrics & Ophthalmology, Neonatal-Perinatal Medicine Clinical & Translational Research Labs, Department of Pediatrics, Division of Neonatal-Perinatal Medicine, State University of New York, Downstate Medical Center, 450 Clarkson Avenue, Room BSB 4-22, Box 49, Brooklyn, NY 11203, USA;
kbeharry@downstate.edu.

Submitted: July 26, 2014
Accepted: February 2, 2015

Citation: Jivabhai Patel S, Bany-Mohammed F, McNally L, et al. Exogenous superoxide dismutase mimetic without scavenging H_2O_2 causes photoreceptor damage in a rat model for oxygen-induced retinopathy. *Invest Ophthalmol Vis Sci*. 2015;56:1665–1677. DOI:10.1167/iovs.14-15321

Purpose. Frequent, brief intermittent episodes of hypoxia (IH) during hyperoxia increase reactive oxygen species in the immature retina with compromised antioxidant systems, thus leading to oxygen-induced retinopathy (OIR). We examined the hypothesis that early exposure to a mimetic of superoxide dismutase (SOD), the first line of defense against oxidative stress, will decrease IH-induced reactive oxygen species (ROS) and prevent severe OIR in our rat model.

Methods. To test this hypothesis, newborn rats (P0) were exposed to IH consisting of alternating cycles of 50% O_2 with brief hypoxia (12% O_2) until P14 during which they were treated with a single daily intraperitoneal (IP) dose of MnTBAP (a SOD mimetic) at 1.0, 5.0, or 10.0 mg/kg on P0, P1, and P2. A saline-treated group served as vehicle controls. Groups were analyzed following IH at P14 or allowed to recover in room air (RA) until P21. Control littermates were raised in RA with all conditions identical except for inspired O_2. Ocular assessment of OIR severity, oxidative stress, angiogenesis, antioxidant activity, and oxidative phosphorylation (OXPHOS) were conducted at P14 and P21.

Results. Collectively, the data show increased oxidative stress and angiogenesis with MnTBAP, which was associated with photoreceptor damage, retinal characteristics consistent with severe OIR, and changes in genes regulating OXPHOS.

Conclusions. In the setting of IH, the use of exogenous SOD mimetics must be combined with H_2O_2 scavengers in order to prevent photoreceptor damage and severe OIR.

Keywords: antioxidants, intermittent hypoxia, oxygen-induced retinopathy, retina

Retinopathy of prematurity (ROP) is a leading cause of childhood blindness worldwide. Approximately 16,000 preterm infants develop ROP annually in the United States, and with improving neonatal care, the incidence is rising in developing countries.[1] Since the 1940s, oxygen has been implicated in the pathogenesis of ROP. With significant advances in the management of oxygen exposure, there was an initial decline in the incidence of ROP. However, with advancing neonatal care and survival of extremely low-gestational-age neonates (ELGANs), a second epidemic of ROP has emerged as a significant morbidity in the neonatal intensive care unit,[2,3] specifically affecting ELGANs who experience frequent, brief arterial oxygen desaturations, or apneas. The etiology of this "new" form of ROP is multivariate and complex, and involves hypersensitivity of the immature retina to changes in oxygen.

Choroidal oxygen delivery to the retina is tightly regulated.[4] Immature retinas of ELGANs have an impaired ability to limit oxygen delivery. This, in combination with immature antioxidant systems[5] and the abundance of polyunsaturated fatty acids and high metabolic rate, makes the retina particularly susceptible to oxidative damage.[6] Human and animal studies have demonstrated that variable oxygen is a key factor involved in the development of ROP.[2,7–10] Specifically, those infants experiencing the greatest fluctuations in their PaO_2 seem to be at higher risk for developing threshold ROP.[7] The pathophysiology of ROP is currently viewed as occurring in two successive phases. Phase 1 starts with suppression of retinal vascular growth upon exposure of the immature retina to oxygen during supplemental oxygen therapy following preterm birth (vaso-obliteration). Vaso-obliteration causes hypoxia of the immature retinal vasculature and release of growth factors that lead to abnormal retinal vascular overgrowth in phase 2 (vasoproliferation).[3] Studies in our laboratory have shown that these two phases occur simultaneously in our oxygen-induced retinopathy (OIR) model that simulates frequent, brief oxygen desaturations experienced by ELGANs.[11,12] What is not known are the roles of the reactive oxygen species (ROS), antioxidants, and oxidative phosphorylation (OXPHOS) in this model of "new ROP."

The mitochondria are the main consumers of oxygen and producers of ROS and antioxidants. Reactive oxygen species may exert their damage directly, or they may act as molecular signals upregulating the genes involved in angiogenesis (e.g., VEGF).[13] To date, the only significant work involving the mitochondria and OIR has been conducted by Penn et al.,[14] who demonstrated

reduced avascular area of the retina with exogenous treatment with liposomal manganese superoxide dismutase (MnSOD). This study was done in rat pups exposed to constant hyperoxia, 80%. However, since ELGANs experience IH in the order of minutes, we used a unique model of brief IH to test the hypothesis that early exposure to superoxide dismutase (SOD), a potent superoxide anion scavenger, will decrease IH-induced ROS and prevent severe OIR in our rat model simulating apnea and brief arterial oxygen desaturations in ELGANs. To test our hypothesis, we used MnTBAP, a SOD mimetic and peroxynitrite scavenger. Our objectives were to examine the dose–response effects of MnTBAP on the development of severe OIR in our rat model; to assess the effect of MnTBAP on ocular biomarkers of oxidative stress, angiogenesis, and antioxidant activity; and to determine the mRNA expression of VEGF signaling genes and genes regulating OXPHOS in the retina during the two phases of ROP, vaso-obliteration (phase 1, P14) and vasoproliferation/reoxygenation (phase 2, P21).

Materials and Methods

All experiments were conducted according to the ARVO Statement for the Use of Animals in Ophthalmic and Visual Research.

Experimental Design

Timed-pregnant Sprague-Dawley rats were purchased from Charles River Laboratories (Wilmington, MA, USA). Within 2 to 3 hours of birth, newborn rat pups delivered on the same day were pooled and randomly assigned to expanded litters of 18 pups/litter. The expanded litter size was used to simulate the relative postnatal malnutrition ELGANs experience, which increases their risk for ROP. Each pup was weighed and measured for linear growth (crown-to-rump length in centimeters). The IH profile of 50%/12% O_2 was as previously described.[11] This design has been shown to produce a severe form of OIR in neonatal rats. A total of 16 groups were studied, and drug or placebo saline was administered as a 3-day consecutive treatment on P0, P1, and P2. Groups 1 to 4 were exposed to hyperoxia/hypoxia cycling from P1 to P14 and received intraperitoneal (IP) injections on P0, P1, and P2 prior to euthanasia on P14 (phase I): group 1, MnTBAP 1 mg/kg/d; group 2, MnTBAP 5 mg/kg/d; group 3, MnTBAP 10 mg/kg/d; and group 4, equivalent-volume saline. Groups 5 to 8 were exposed to hyperoxia/hypoxia cycling from P1 to P14, received similar MnTBAP doses on P0, P1, and P2, and then were placed in room air (RA) from P14 to P21 (phase II). Groups 9 to 16 served as RA controls. Groups 9 to 12 received similar MnTBAP doses P0, P1, and P2 and remained in RA from P0 to P14; and groups 13 to 16 received similar MnTBAP doses on P0, P1, and P2 and remained in RA from P0 to P21. The doses of MnTBAP were based on previous reports showing that IP injections of 5 mg/kg/d prolonged the life span of neonatal mice with nullizygous SOD2.[15,16]

Sample Collection

Both eyes from nine male and nine female pups in each group were enucleated and rinsed in ice-cold phosphate-buffered saline (PBS; pH 7.4) on ice. The vitreous fluid (VF) was aspirated and processed as previously described.[11,12] Vitreous fluid was pooled for a total of six samples per group (three males and three females). None of the VF samples were contaminated with blood. The retinas were then excised and processed as previously described.[11,12] Retinas were pooled to obtain enough samples for enzyme-linked immunosorbent assay (ELISA) and quantitative polymerase chain reaction (qPCR) assays. Retinas were also assessed using fluorescein-dextran, adenosine diphosphatase (ADPase), and hematoxylin and eosin (H&E) staining.

Retinal Fluorescein–Dextran Perfusion

Fluorescein–dextran perfusion was carried out as previously described.[11,12] To determine retinal vascular development, computer-digitized images of fluorescein–dextran-stained retinas were examined. Images are presented at ×10 magnification.

Retinal ADPase Staining

Adenosine diphosphatase staining of the retinas and computer imaging were carried out as previously described.[11,12,17] Digital images of the whole flattened, stained retinas were captured at ×4 magnification for scoring. Images were saved using the SPOT software (Diagnostic Instruments, Inc., Sterling Heights, MI, USA), Olympus BH-2 microscope (McBain Instruments, Chatsworth, CA, USA), and Dell Optiplex GX280 computer (Dell Computer Corporation, Dallas, TX, USA). Images of the ADPase-stained and fluorescein–dextran-stained retinas are presented at ×10 magnification. All images were assessed by an ophthalmology pathologist.

Quantification of Retinal Neovascularization and Retinal Scoring

Scoring of the retinas was conducted by the same individuals who carried out the staining and imaging. Therefore, scoring was not masked despite deidentification of the slides during the scoring process. Neovascularization was determined as calculated area (μm^2) of retinal overgrowth extending beyond the avascular zone into the ciliary body in each quadrant of the retinal flat mounts (total 32 measurements/group). Each quadrant was divided into three equal parts to represent 3, 6, 9, and 12 clock hours. The area was outlined on the retinal images using the region selection tool of the image analysis software (SPOT), and the ratio of avascular to vascular areas was quantified. For retinal scoring, we used a modified version of the scoring system developed by Higgins et al.[18] The scoring criteria included vascular tufts, retinal overgrowth (vessels growing beyond the avascular zone and into the ciliary body), retinal hemorrhage, vessel tortuosity, and persistence of hyaloid vessels (this criterion was added because persistent hyaloid vessels at P14 and P21 are recruited, and it is usually indicative of neovascularization in our model). For scoring, each retina was divided into 12 equally sized sections representing the "clock hours." A score of 0 was given if none of the characteristics were found in any of the clock hours; a score of 1 was given if found in <3 clock hours; a score of 2 was given if found in 3 to 5 clock hours; a score of 3 was given if found in 6 to 8 clock hours; and a score of 4 was given found in 9 to 12 clock hours. The retinopathy score was calculated by the sum of points for each criterion and divided by the number of retinas for an average score. The maximum score was 24. A score of >12 was considered severe OIR.[11]

Oxidative Stress and Lipid Peroxidation

Isoprostanes are prostanoid derivatives that are produced by the nonenzymatic peroxidation of arachidonic acid through ROS. 8-Isoprostane, or 8-isoPGF$_{2\alpha}$, is commonly studied and is abundantly generated in vivo during oxidative stress and lipid peroxidation. To establish ocular oxidative stress, levels of 8-isoPGF$_{2\alpha}$ were determined in the undiluted VF and retinal homogenates using commercially available enzyme immunoassay kits from Assay Designs, Inc. (Ann Arbor, MI, USA)

Investigative Ophthalmology & Visual Science

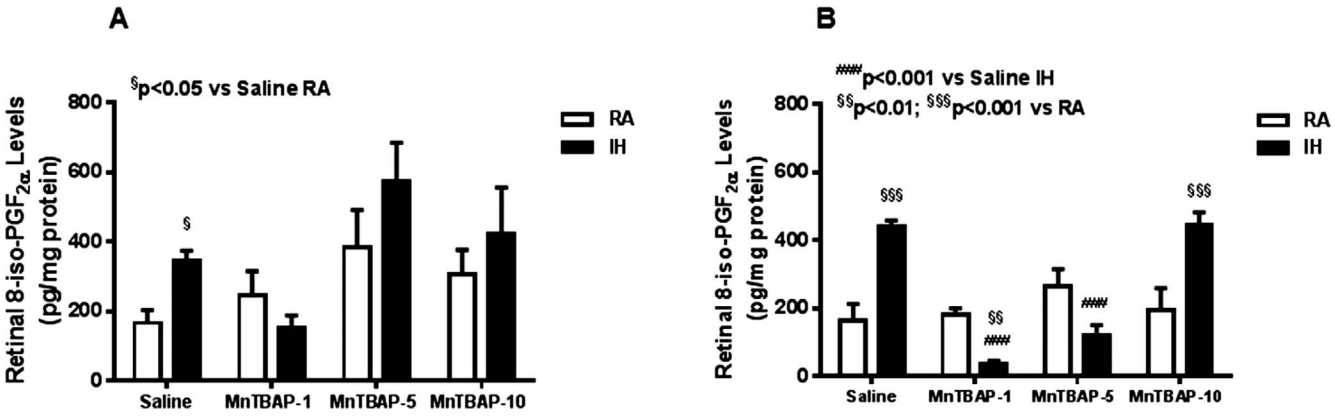

Figure 1. Dose–response effects of MnTBAP on retinal 8-isoPGF$_{2\alpha}$ in neonatal rats at P14 (**A**) and P21 (**B**). Animals were treated with a single IP dose of either 1, 5, or 10 mg/kg on P0, P1, and P1. Animals were exposed to intermittent hypoxia (IH) from P0 to P14 (**A**). Animals studied at P21 were placed in room air (RA) from P14 to P21. Room air littermates were raised in RA from P0 to P14 or P0 to P21 and treated with similar doses of MnTBAP or equivalent-volume saline. To compare data among the RA (*) or IH (#) groups (saline versus MnTBAP treated), one-way ANOVA was employed for normally distributed data, and Kruskal-Wallis test was used for nonnormally distributed data. To compare data between RA and IH groups (§) for each treatment, unpaired *t*-test was employed for normally distributed data and Mann-Whitney *U* tests were used for nonnormal data. Data are presented as mean ± SEM ($n = 6$ samples/groups).

according to the manufacturer's protocol. Levels in the retinal homogenates were standardized using total cellular protein levels according to the Bradford method (BioRad Laboratories, Hercules, CA, USA).

Antioxidant Activity

Catalase, SOD, and glutathione peroxidase (GPX) activities were determined in undiluted VF and retinal homogenates using commercially available assay kits from Cayman Chemicals (Ann Arbor, MI, USA) as previously described.[17] Levels in the retinal homogenates were standardized using total cellular protein levels according to the Bradford method (BioRad Laboratories).

VEGF and sVEGFR-1

On the day of the assay, retinas were homogenized on ice, centrifuged at 2370*g* at 4°C for 20 minutes. Vascular endothelial growth factor and soluble vascular endothelial growth factor receptor (sVEGFR)-1 levels were determined in undiluted VF and retinal homogenates using commercially available sandwich immunoassay kits for rat/mouse from R&D Systems (Minneapolis, MN, USA). Levels in the retinal homogenates were standardized using total cellular protein levels according to the Bradford method (BioRad Laboratories).

Retinal H&E Staining

Eyes were enucleated, rinsed in PBS, fixed in Hartmann's fixative, and sent to New York University Experimental Pathology Histology Core Laboratory, New York, New York for H&E staining. During embedding and sectioning, the eyes were oriented with the cornea horizontal to the optic nerve and the optic nerve visible in the sections. Images were taken at the central retina and captured at ×40 magnification using an Olympus BX53 microscope, DP72 digital camera, and CellSens imaging software (Olympus, Center Valley, PA, USA), attached to a Dell Precision T3500 computer (Dell, Round Rock, TX, USA). All images were assessed by an ophthalmology pathologist.

Real-Time Polymerase Chain Reaction

Total retinal RNA was extracted as previously described.[11,12,17] To identify genes that are affected by MnTBAP in IH, real-time PCR arrays were carried out in duplicate using the rat mitochondrial energy metabolism and rat VEGF Signaling PCR array systems (SABiosciences, Frederick, MD, USA) using a BioRad Laboratories IQ5 real-time instrument.

Statistical Analysis

One-way analysis of variance (ANOVA) was used to determine differences among the groups for normally distributed data, and Kruskal-Wallis test was used for nonnormally distributed data following Bartlett's test for equality of variances. Post hoc analysis was performed using the Tukey, Bonferroni, and Student-Newman-Keuls tests for significance. To compare data between RA and IH groups, unpaired *t*-test was employed for normally distributed data and Mann-Whitney *U* tests were used for nonnormal data following Levene's test for equality of variances. The Mann-Whitney *U* test was used to analyze the scoring data. Significance was set at $P < 0.05$, and data are reported as mean ± SEM. All analyses were two-tailed and performed using SPSS version 16.0 (SPSS, Inc., Chicago, IL, USA). Graphs were prepared using GraphPad Prism ver. 5 software (GraphPad, San Diego, CA, USA).

Results

No Long-Term Effects of MnTBAP on Somatic Growth

The groups exposed to IH and treated with MnTBAP were generally heavier than RA controls. However, MnTBAP did not have long-lasting effects on growth, as it appeared to preserve body weight accretion closer to the time of administration (data not shown).

High MnTBAP Doses Increase Oxidative Stress

Retinal 8-isoPGF$_{2\alpha}$ levels were measured as a marker for oxidative stress. At P14, retinal 8-isoPGF$_{2\alpha}$ levels were significantly higher in the saline-treated IH group compared to RA. No similar increases were noted with MnTBAP (Fig. 1A). At P21, a more profound elevation in retinal 8-isoPGF$_{2\alpha}$ levels was noted in the saline-treated IH group compared to RA. This increase was attenuated with the 1 and 5 mg/kg doses of

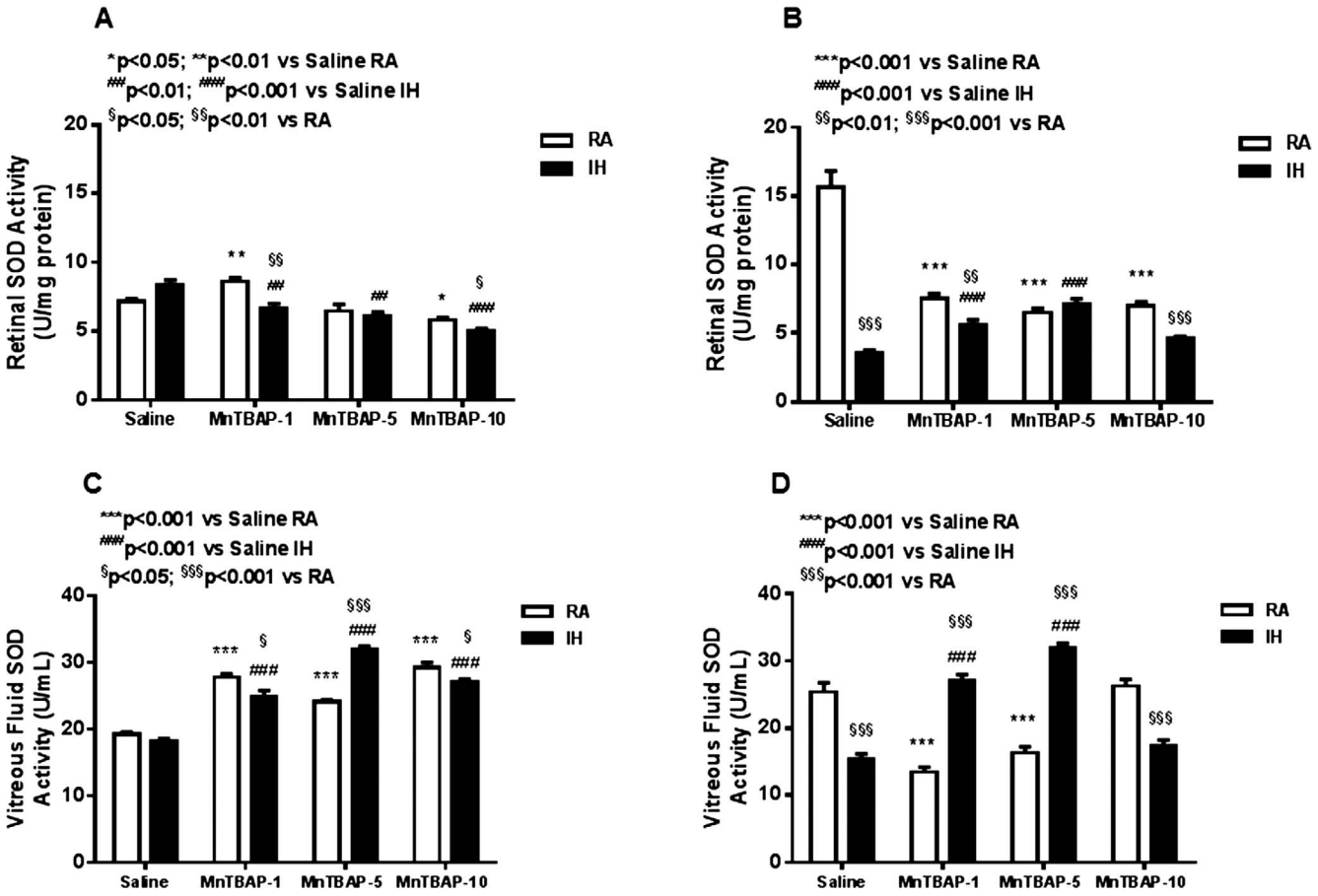

FIGURE 2. Dose–response effects of MnTBAP on retinal SOD activity in neonatal rats at P14 (**A**) and P21 (**B**) and vitreous fluid SOD at P14 (**C**) and P21 (**D**). Treatment groups are as described for Figure 1. Statistical analyses were conducted as described for Figure 1. Data are presented as mean ± SEM ($n = 6$ samples/group).

MnTBAP. On the other hand, the 10 mg/kg MnTBAP dose significantly increased retinal 8-isoPGF$_{2\alpha}$ levels (Fig. 1B) in the IH group. There was no effect of MnTBAP on 8-isoPGF$_{2\alpha}$ in the RA-treated groups.

MnTBAP Increases Vitreous Fluid SOD

At P14 there was a decrease in retinal SOD activity with progressively larger MnTBAP doses (Fig. 2A) in both RA and IH groups. At P21, retinal SOD activity in saline-treated IH control was significantly lower than in RA (Fig. 2B). MnTBAP treatment in RA uniformly suppressed retinal SOD activity. Conversely, treatment with the lower doses in IH increased retinal SOD levels, but not with the highest dose. In the VF, there was a more robust SOD response to MnTBAP resulting in higher levels with all doses in RA and IH compared to saline treatment in RA and IH at P14 (Fig. 2C). Similar to the changes in retinal tissue, at P21, the decrease in SOD in response to IH persisted. Treatment with 1 and 5 mg/kg MnTBAP in RA decreased VF SOD activity, but not 10 mg/kg. The opposite was true for treatment in IH (Fig. 2D). No differences in catalase and GPX were detected among the groups (data not shown).

MnTBAP Increases VEGF

At P14, exposure to IH increased retinal VEGF levels compared with RA. Treatment with MnTBAP further increased VEGF level in all treatment groups, but the effect was greater with the lower doses (Fig. 3A). At P21, the increase in retinal VEGF was sustained with IH with no amelioration by MnTBAP treatment. Of note was the increase in VEGF level with MnTBAP treatment in RA groups (Fig. 3B). Vitreous fluid VEGF was lower in the saline-treated IH group and in the group that received the highest dose of MnTBAP. An opposite effect occurred with the two lower doses of MnTBAP (Fig. 3C). At P21, VEGF levels were higher in both the saline-treated and 10 mg/kg MnTBAP groups (Fig. 3D). At P14, retinal sVEGFR-1 was lower only with MnTBAP 5 mg/kg treatment in IH (Fig. 4A). At P21, retina sVEGFR-1 levels were higher in the saline-treated IH group. MnTBAP treatment resulted in higher sVEGFR-1 levels in RA groups. On other hand, MnTBAP treatment at 5 and 10 mg/kg decreased retinal sVEGFR-1 levels in IH compared to RA groups (Fig. 4B). In the VF, sVEGFR-1 levels were lower with MnTBAP treatment in RA (Fig. 4C). At P21, VF sVEGFR-1 was lower with 10 mg/kg MnTBAP treatment in RA and higher with treatment in IH (Fig. 4D).

High Doses of MnTBAP Cause Severe OIR

The avascular-to-vascular ratios are presented in Table 1. At P14, the mean ratio was higher in the saline-treated IH group (4.8 ± 0.47, $P < 0.001$) compared to the corresponding RA group (3.1 ± 0.31). The ratio was significantly lower with 10 mg/kg MnTBAP treatment in RA (1.92 ± 0.21, $P < 0.01$) compared to saline (3.1 ± 0.31). Similar reductions were noted with the 5 mg/kg (2.0 ± 0.21, $P < 0.01$) and 10 mg/kg (1.93 ± 0.21, $P < 0.01$) doses when administered during IH compared to saline treatment in IH (4.8 ± 0.47). At P21, the

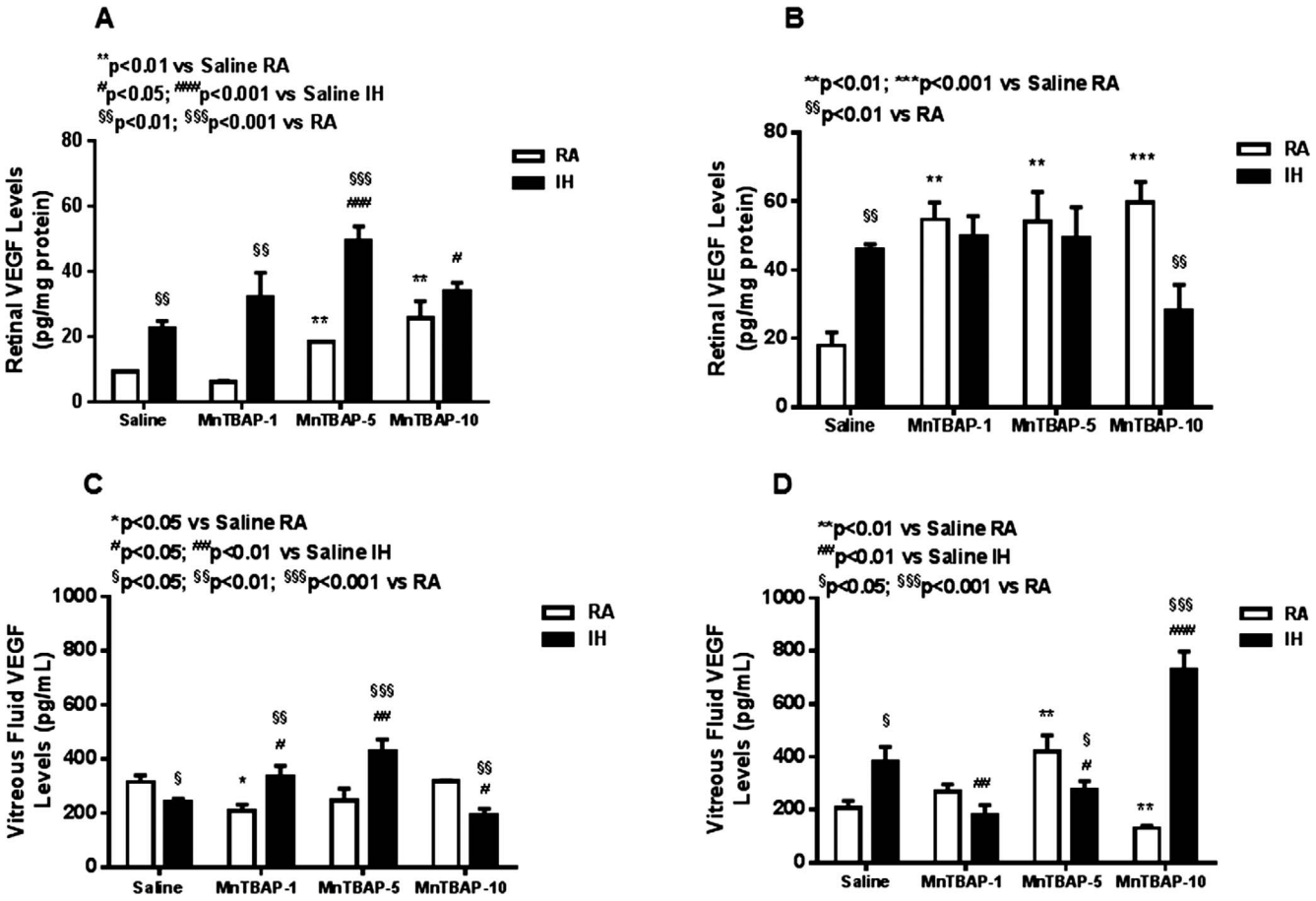

FIGURE 3. Dose–response effects of MnTBAP on retinal VEGF in neonatal rats at P14 (**A**) and P21 (**B**) and vitreous fluid VEGF at P14 (**C**) and P21 (**D**). Treatment groups are as described for Figure 1. Statistical analyses were conducted as described for Figure 1. Data are presented as mean ± SEM ($n = 6$ samples/group).

avascular-to-vascular ratio was reduced with 1 mg/kg (1.1 ± 0.09, $P < 0.01$) and 5 mg/kg (0.72 ± 0.05, $P < 0.01$) doses compared to saline (3.0 ± 0.24) treatment in RA. In IH, only the 5 mg/kg dose effectively reduced the avascular-to-vascular ratio (0.85 ± 0.1, $P < 0.01$) compared to saline (2.3 ± 0.23). The average retinal scores are presented in Table 2. At P14, retinal scores were increased with 10 mg/kg MnTBAP treatment in RA ($P < 0.01$) compared to saline. Treatment with MnTBAP in IH did not significantly improve the retinal scores. At P21, retinal scoring for vascular pathology revealed that 75% of the retinal flat mounts in the saline-treated and IH group scored >12. Similar findings were noted with the highest dose of MnTBAP.

Figures 5 and 6 show a single representative retinal flat mount from each group at P14 and P21, respectively. Specific areas have been magnified and presented in the Supplementary Material for the IH groups only. The retinas were stained with ADPase (brown) and fluorescein-dextran (green). The upper images represent the RA saline (Figs. 5A, 6A), 1 mg/kg MnTBAP (Figs. 5B, 6B), 5 mg/kg MnTBAP (Figs. 5C, 6C), and 10 mg/kg MnTBAP (Figs. 5D, 6D) groups. The lower images represent the corresponding IH groups. At P14, RA images show early vascular dilation (Fig. 5B, arrow), moderate vascular dilation (Fig. 5C, arrow), and vessel dilation and neovascularization in loops (Fig. 5D, arrow). The corresponding fluorescein images confirm the findings. The IH images show mild vascular dilation and fluorescein leakage (Fig. 5E); moderate vascular dilation (Fig. 5F); moderate vascularization and capillary dropout (Fig. 5G); and moderate vascularization, advanced capillary dropout, and fluorescein leakage (Fig. 5H). At P21, RA images show moderate capillary dropout (Fig. 6B), early neovascularization (Fig. 6C), and neovascularization (Fig. 6D). The IH images show retinal hemorrhages and vascular leakage (Fig. 6E); retinal hemorrhages, neovascularization, and focal vascular leakage (Fig. 6F); capillary dropout and moderate vascular dilation and neovascularization (Fig. 6G); and retinal hemorrhages and neovascularization (Fig. 6H). Treatment with MnTBAP did not appreciably reduce the vascular pathology, resulting in similar extents of retinal vascular overgrowth and retinal scoring (Figs. 6F–H). Of concern was the evidence for vascular pathology with MnTBAP treatment in RA groups.

High Doses of MnTBAP Cause Photoreceptor Damage

Figure 7 shows the retinal layers stained with H&E. The layers are labeled in Figure 7A only (NFL, nerve fiber layer; GCL, ganglion cell layer; IPL, inner plexform layer; INL, inner nuclear layer; OPL, outer plexiform layer; ONL, outer nuclear layer; P, photoreceptors; C, choroid). Figures 7A through 7D represent saline, MnTBAP 1 mg/kg, MnTBAP 5 mg/kg, and MnTBAP 10 mg/kg treatment in RA at P14, respectively. Figures 7E and 7F are the corresponding IH groups. Figures 7I through 7L are the corresponding RA groups at P21, and Figures 7M through 7P are the corresponding IH groups at P21. For all groups the inner retina is oriented to the right. Images show mild NFL vacuolization and/or loss (arrow, Fig. 7B); moderate NFL vacuolization and/or loss (Fig. 7C); severe NFL

Investigative Ophthalmology & Visual Science

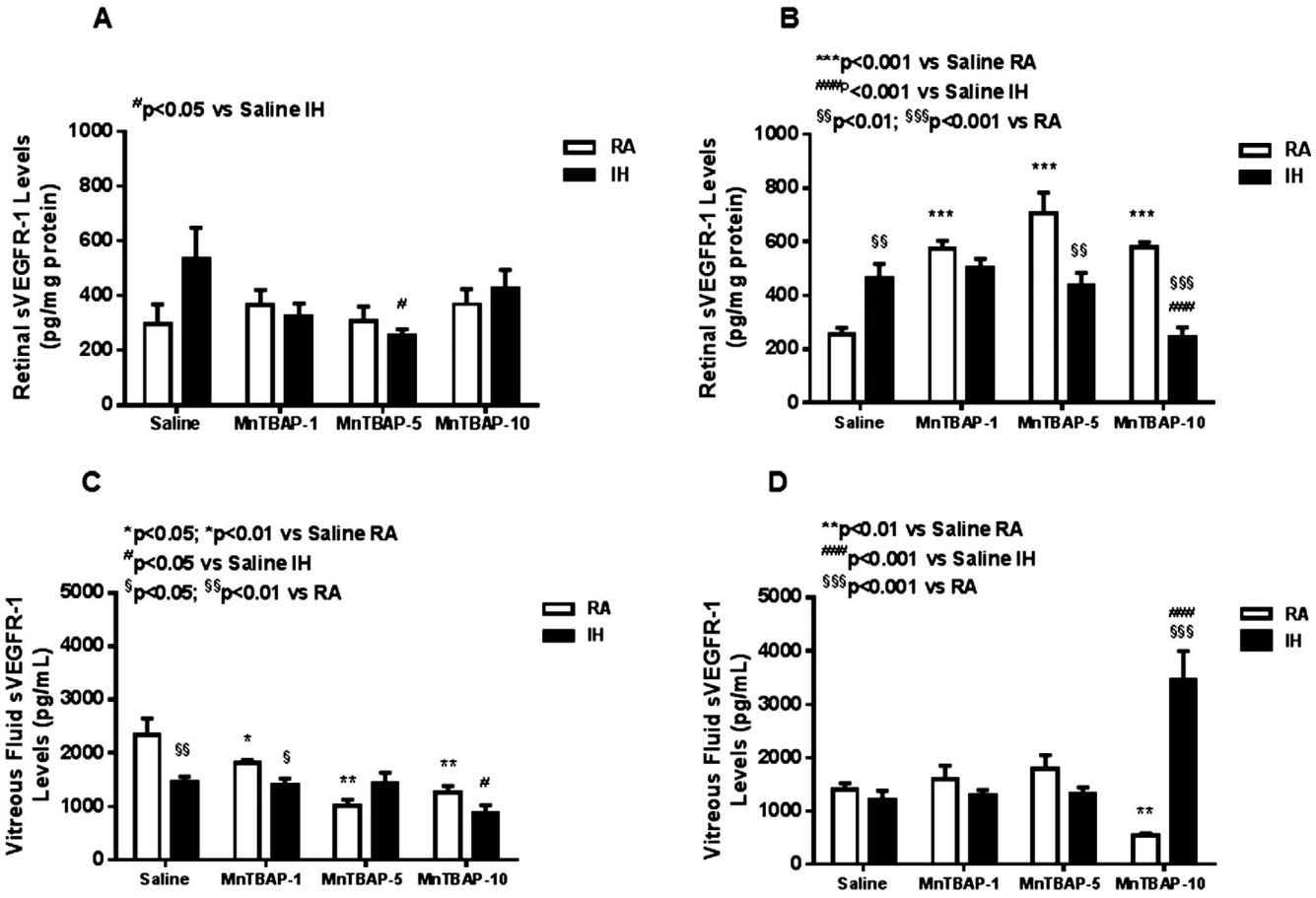

FIGURE 4. Dose–response effects of MnTBAP on retinal sVEGFR-1 in neonatal rats at P14 (**A**) and P21 (**B**) and vitreous fluid sVEGFR-1 at P14 (**C**) and P21 (**D**). Treatment groups are as described for Figure 1. Statistical analyses were conducted as described for Figure 1. Data are presented as mean ± SEM ($n = 6$ samples/group).

vacuolization and/or loss, ganglion cell nuclear atrophy, and photoreceptor degeneration (arrow, Fig. 7E); degeneration of NFL and increased blood vessel caliber (arrow, Fig. 7F); degeneration of NFL and severe photoreceptor damage (arrows, Fig. 7H); moderate NFL vacuolization and/or loss (arrow, Fig. 7J); moderate NFL vacuolization and/or loss, dilation of the choroidal vasculature; and photoreceptor degeneration (arrows, Fig. 7K); severe NFL vacuolization and/or loss, ganglion cell nuclear atrophy, and photoreceptor degeneration (arrow, Fig. 7L); neovascularization and hemorrhage (arrows, Fig. 7M); degeneration of NFL, increased blood vessel caliber and wall thickness, retinal folding, photoreceptor

TABLE 1. Ratio of Avascular to Vascular Area in Retinal Flat Mounts From 14- and 21-Day-Old Neonatal Rats Exposed to Intermittent Hypoxia and Treated With MnTBAP ($n = 8$ Eyes/Group, 4 Males and 4 Females)

Clock Hours	Saline RA	Saline O_2	MnTBAP 1 mg, RA	MnTBAP 1 mg, O_2	MnTBAP 5 mg, RA	MnTBAP 5 mg, O_2	MnTBAP 10 mg, RA	MnTBAP 10 mg, O_2
P14:								
3	0.80 ± 0.06	0.91 ± 0.12	0.66 ± 0.05	0.66 ± 0.12	0.46 ± 0.04	0.55 ± 0.06	0.52 ± 0.09	0.54 ± 0.11
6	0.87 ± 0.11	1.1 ± 0.14	0.86 ± 0.13	0.93 ± 0.41	0.51 ± 0.04	0.41 ± 0.04	0.50 ± 0.07	0.47 ± 0.04
9	0.70 ± 0.07	1.81 ± 0.1	0.76 ± 0.12	0.83 ± 0.24	0.73 ± 0.21	0.54 ± 0.05	0.49 ± 0.08	0.42 ± 0.08
12	0.76 ± 0.07	1.00 ± 0.1	0.72 ± 0.13	0.81 ± 0.15	0.49 ± 0.05	0.58 ± 0.17	0.41 ± 0.04	0.50 ± 0.06
Total	3.1 ± 0.31	4.8 ± 0.47*	3.0 ± 0.27	3.2 ± 0.72	2.2 ± 0.25	2.0 ± 0.21†	1.92 ± 0.21‡	1.93 ± 0.21†
P21:								
3	0.84 ± 0.05	0.66 ± 0.05	0.23 ± 0.02	0.64 ± 0.06	0.18 ± 0.02	0.27 ± 0.03	0.94 ± 0.1	1.2 ± 0.07
6	0.84 ± 0.09	0.58 ± 0.05	0.29 ± 0.03	0.37 ± 0.05	0.19 ± 0.04	0.20 ± 0.02	0.86 ± 0.14	0.53 ± 0.06
9	0.73 ± 0.05	0.53 ± 0.09	0.28 ± 0.04	0.72 ± 0.14	0.20 ± 0.04	0.23 ± 0.03	0.64 ± 0.15	0.54 ± 0.12
12	0.63 ± 0.05	0.54 ± 0.04	0.25 ± 0.04	0.57 ± 0.07	0.15 ± 0.02	0.15 ± 0.04	0.77 ± 0.11	0.35 ± 0.06
Total	3.0 ± 0.24	2.3 ± 0.23	1.1 ± 0.09‡	2.3 ± 0.23	0.72 ± 0.05‡	0.85 ± 0.1†	3.2 ± 0.50	2.6 ± 0.68

* $P < 0.01$ versus RA.
† $P < 0.01$ versus saline IH.
‡ $P < 0.01$ versus saline RA.

Table 2. Retinopathy Scores From 14- and 21-Day-Old Neonatal Rats Exposed to Intermittent Hypoxia and Treated With MnTBAP ($n = 8$ Eyes/Group, 4 Males and 4 Females; Maximum Score = 24)

Measured Variables	Saline RA	Saline O_2	MnTBAP 1 mg, RA	MnTBAP 1 mg, O_2	MnTBAP 5 mg, RA	MnTBAP 5 mg, O_2	MnTBAP 10 mg, RA	MnTBAP 10 mg, O_2
P14:								
Vascular tufts	0	3	2	3	0	2	2	2
Extraretinal neovascularization	0	0	0	1	0	1	2	0
Vessel tortuosity	0	4	0	3	2	2	2	2
Hemorrhage	0	4	2	2	1	2	2	3
Dilated vessels	0	3	0	2	0	2	2	3
Persistence of hyaloid vessels	2	2	0	3	3	2	3	4
Average score	2	16	4	14	6	11	13*	14
P21:								
Vascular tufts	0	4	0	2	1	3	0	4
Extraretinal neovascularization	0	4	0	3	1	1	0	4
Vessel tortuosity	0	4	1	3	1	3	2	4
Hemorrhage	0	4	0	3	1	4	1	4
Dilated vessels	0	4	1	2	0	3	2	4
Persistence of hyaloid vessels	1	4	2	2	3	2	1	4
Average score	1	24	4	15	7	16	6	24

* $P < 0.01$ versus saline RA.

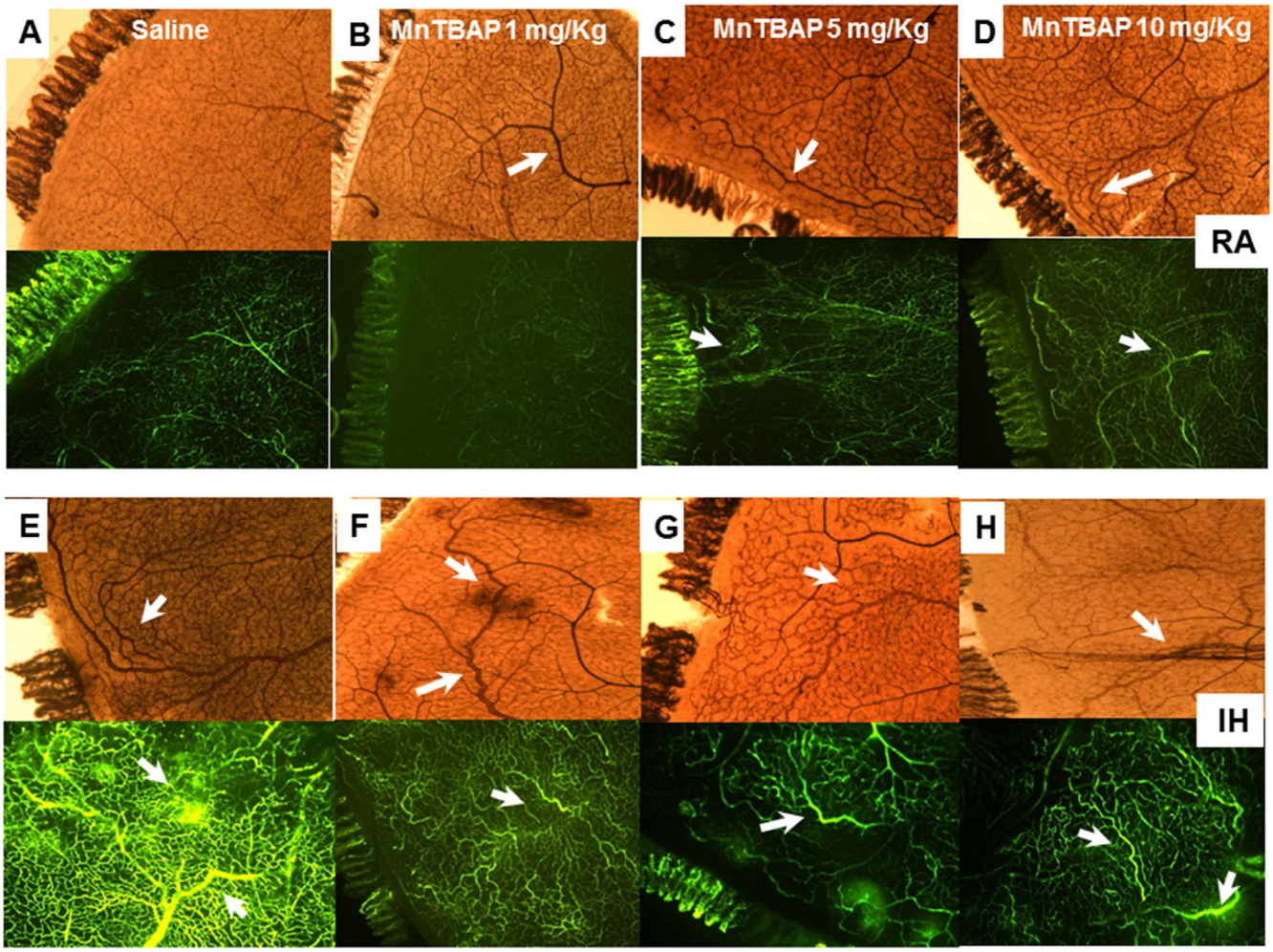

Figure 5. Representative retinal flat mounts showing ADPase- and fluorescein–dextran-stained retinas from 14-day-old rat pups exposed to RA (**A**–**D**) and IH (**E**–**H**). (**A**, **E**) Saline (control); (**B**, **F**) 1 mg/kg MnTBAP; (**C**, **G**) 5 mg/kg MnTBAP; (**D**, **H**) 10 mg/kg MnTBAP. Images are at ×10 magnification.

Investigative Ophthalmology & Visual Science

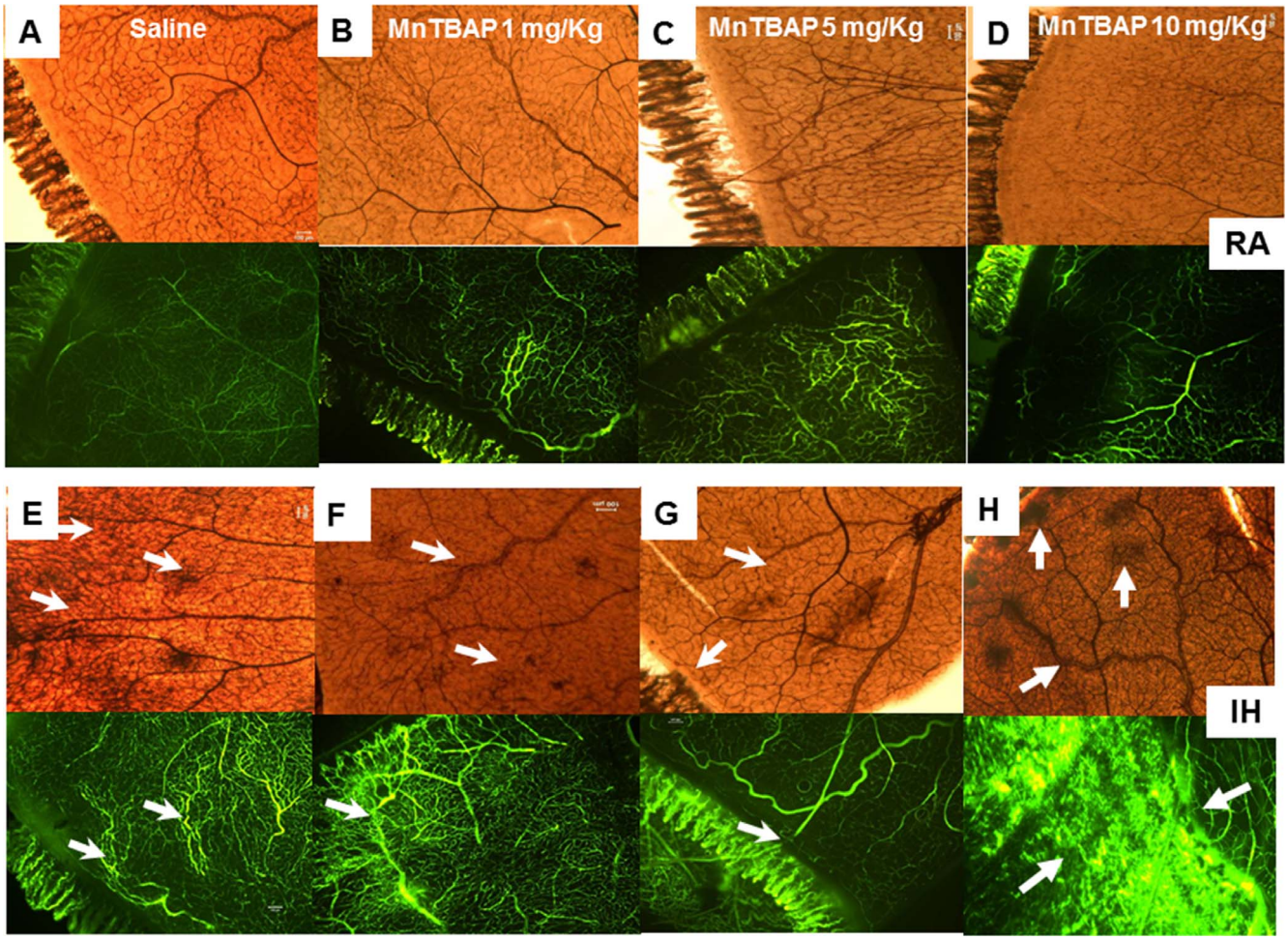

Figure 6. Representative retinal flat mounts showing ADPase- and fluorescein–dextran-stained retinas from 21-day-old rat pups exposed to RA (**A**–**D**) and reoxygenation from IH (**E**–**H**). (**A**, **E**) saline (control); (**B**, **F**) 1 mg/kg MnTBAP; (**C**, **G**) 5 mg/kg MnTBAP; and (**D**, **H**) 10 mg/kg MnTBAP. Images are at ×10 magnification.

degeneration, and ONL hemorrhage (arrows, Fig. 7N); marked degeneration of NFL, increased blood vessel caliber and wall thickness, and neovascularization violating the ILM (arrow, Fig. 7O); neovascularization of retina posterior to the level of OPL, degeneration of the NFL, and severe choroidal hemorrhage with possible retinal detachment (arrows, Fig. 7P).

VEGF and OXPHOS Gene Profiling

Table 3 represents the retinal VEGF signaling genes taken from a panel of 84 genes. Data are fold regulation compared to saline-treated RA controls. At P14, there were only mild changes in the VEGF signaling pathway genes with MnTBAP treatment in RA and IH. However, at P21, all genes were upregulated in the saline-treated IH group several-fold compared to saline-treated RA controls. A less robust upregulation (downregulation compared to saline-treated IH group) was noted with MnTBAP treatment. Table 4 shows expression of retinal OXPHOS genes taken from a panel of 84 genes. Data are fold regulation compared to saline-treated RA controls. At P14, in the saline IH group, only *Uqcrb* (involved in complex III) was upregulated compared to RA. With regard to MnTBAP treatment, *ATPSF0E* (involved in complex V) was 457-fold downregulated with 1 mg/kg MnTBAP in the IH group. Similar effects were noted with the 10 mg/kg dose in RA (89-fold) and IH (115-fold) groups. *Cox4i1* and *Cox8c* (involved in complex IV) were also downregulated 84-fold and 16-fold, respectively, with the 1.0 mg/kg MnTBAP dose in IH groups. In contrast, *Uqcrb* (involved in complex III) was robustly upregulated in all groups compared to control. At P21, IH caused significant downregulation of *ATPSF0E* (18-fold), *Cox4i1* (27-fold), *Cox8a* (6-fold), and *Ndufab1* (31-fold). MnTBAP treatment in the saline-treated IH groups resulted in attenuation of this effect; *ATPSF0E* was upregulated 9-fold with MnTBAP treatment of 1 mg/kg, 1.4 upregulated with 5 mg/kg dose, and 6.4 upregulated with 10 mg/kg dose. MnTBAP treatment resulted in similar attenuation of IH on *Cox4i1*, *Cox8a*, and *Ndufab1*. On the other hand, *Ndufc2* was significantly upregulated in the saline-treated IH group. MnTBAP therapy maintained this upregulation with some additive effect at the 1 mg/kg dose (77-fold versus 63-fold). MnTBAP therapy in RA also caused upregulation of *Ndufc2*. In addition, *Ndufb9* was downregulated with 10 mg/kg MnTBAP treatment in the group recovering from IH. Lastly, *Uqcrb* upregulation noted in the saline-treated IH group at P14 was ameliorated at P21.

Discussion

The present study examined the hypothesis that a SOD mimetic will decrease IH-induced ROS and prevent severe OIR in a rat model simulating frequent, brief IH episodes in ELGANs. We opted to treat the pups only from P0 to P2, which

Investigative Ophthalmology & Visual Science

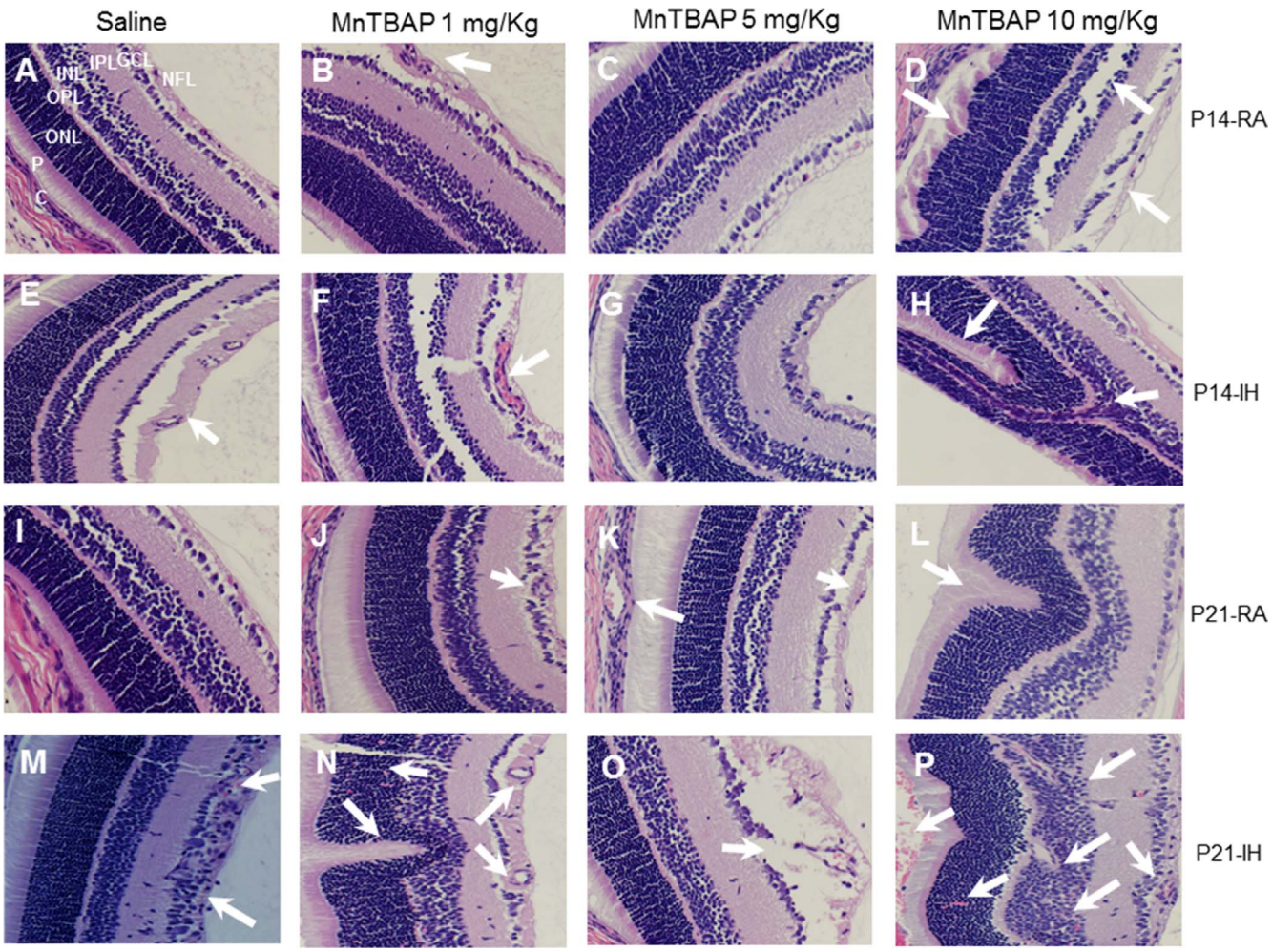

Figure 7. Representative H&E stain of retinal layers from 14-day-old (**A–H**) and 21-day-old (**I–P**) rat pups. Retinal layers are labeled in (**A**) as NFL (nerve fiber layer); IPL (inner plexiform layer); INL (inner nuclear layer); OPL (outer plexiform layer); ONL (outer nuclear layer); P (photoreceptors); C (choroid). (**A–D**) Saline, MnTBAP 1 mg/kg, MnTBAP 5 mg/kg, and MnTBAP 10 mg/kg treatment in RA at P14, respectively; (**E–H**) the corresponding IH groups; (**I–L**) the corresponding RA groups at P21; (**M–P**) the corresponding IH groups at P21. Images are at ×40 magnification.

is equivalent to 3 weeks in human infants, because the first few weeks of life in ELGANs are critical. Recent studies have demonstrated that ELGANs experience chronic IH episodes over the first 4 weeks of postnatal life[19] and that the pattern of IH was associated with a more severe form of ROP,[20] which is consistent with and confirms our previous findings.[11,12] Using this same model we previously showed that IH results in ocular oxidative stress and hydrogen peroxide (H_2O_2) accumulation in the choroid predominantly during the reoxygenation phase.[17] We now show that treatment with a superoxide anion and peroxynitrite scavenger alone, MnTBAP, did not protect the eye against oxidative stress. Instead, increasing doses exacerbated the damage particularly during the reoxygenation phase. Since SOD converts superoxide anion to H_2O_2, this finding suggests that the use of exogenous SOD without catalase and/or GPX may lead to further H_2O_2 accumulation. Ocular H_2O_2 accumulation contributes to photoreceptor damage[21] and angiogenesis via induction of VEGF/VEGFR-1 signaling,[22] thus leading to retinal neovascularization as demonstrated in Figures 5 through 7. While the lower doses of MnTBAP showed a trend toward decreased angiogenesis, it is unlikely that the lower doses will prevent severe OIR as the use of a H_2O_2 scavenger would still be required. Previous studies by Usui et al.[21] showed that although SOD is an important component of the antioxidant defense system of photoreceptors, coexpression with GPX reduced oxidative damage in the retina. The authors concluded that in order to prevent high levels of H_2O_2 in the retina, SOD must be coadministered with a H_2O_2 detoxifying enzyme. Our data support this premise and suggest that parsimonious use of a single, low-dose SOD with a H_2O_2 scavenger may be a more beneficial therapeutic approach.

Reactive oxygen species including superoxide anion, H_2O_2, and peroxynitrite are catalyzed by various antioxidant systems including SOD.[23] Reactive oxygen species are formed in the mitochondria and play an important role in retinal vaso-obliteration in ROP.[24–26] Oxygen fluctuations experienced by preterm infants induce cells to express nicotinamide adenine dinucleotide phosphate (NADPH) oxidase, which leads to ROS and apoptosis of endothelial cells.[6,27] Using a reliable and proven biomarker for oxidative stress, 8-iso-$PGF_{2\alpha}$[28,29] we showed higher levels in the saline- and MnTBAP 10 mg/kg-treated IH groups at P21 or reoxygenation (phase 2). The present findings confirm previous findings[17,30] and highlight the ongoing damage from ROS during reoxygenation and repair. Superoxide dismutase converts superoxide anion to H_2O_2, which is then metabolized by GPX and catalase.[31] Therefore, coadministration with other antioxidants such as

Table 3. Fold Regulation of VEGF Signaling Genes in the Retinas of Neonatal Rats at 14 and 21 Days Postnatal Age (Data Are Compared to Those for Saline-Treated 14-Day or 21-Day RA Littermates)

Genes of Interest	Saline O_2	MnTBAP 1 mg, RA	MnTBAP 1 mg, O_2	MnTBAP 5 mg, RA	MnTBAP 5 mg, O_2	MnTBAP 10 mg, RA	MnTBAP 10 mg, O_2
P14:							
HIF-1α	1.2	1.0	1.0	1.4	1.1	1.2	−1.4
NP-1	1.8	2.8	2.0	2.4	2.4	1.9	4.3
NP-2	1.5	1.5	1.9	2.6	1.6	1.6	1.3
VEGF-A	−1.7	1.7	1.7	1.4	1.9	1.4	2.8
VEGFR-1	−1.6	2.0	1.4	2.0	1.5	1.9	2.5
VEGFR-2	−1.1	1.3	1.2	1.6	1.6	1.4	1.1
VEGFR-3	−1.4	−1.2	−1.1	−1.1	−1.3	−1.2	1.3
P21:							
HIF-1α	1.4	1.7	2.5	2.1	2.0	2.5	1.6
NP-1	173.6	3.4	5.0	6.0	4.8	4.0	2.0
NP-2	118.8	4.5	5.3	9.1	6.0	5.1	6.8
VEGF-A	45.0	2.7	2.9	3.1	3.0	2.5	2.7
VEGFR-1	151.4	3.0	4.0	5.4	4.0	5.2	1.2
VEGFR-2	10.9	3.0	3.5	2.7	3.5	2.8	3.2
VEGFR-3	195.0	1.5	2.3	2.4	2.4	2.0	1.7

All data were corrected using five different housekeeping genes. Genes were selected from a focused panel of 84 genes in the VEGF signaling pathway. Genes were selected from a focused panel of 84 genes in the OXPHOS signaling pathway. Genes of interest are *HIF-1α* (hypoxia-inducible factor-1 alpha), *NP-1* (neuropilin-1), *NP-2* (neuropilin-2), *VEGF-A* (vascular endothelial growth factor A), *VEGFR-1* (VEGF receptor-1), *VEGFR-2* (VEGF receptor-2), *VEGFR-3* (VEGF receptor-3).

catalase and/or GPX may provide more protection.[27] Superoxide dismutase is the first line of defense against oxidative stress in the mitochondria, with MnSOD located in the inner mitochondrial matrix. Neisman et al.[31] showed an improvement in the avascular area when hyperoxia-exposed rats were treated with liposomal SOD. In our study, during phase 1 (vaso-obliteration), retinal SOD activity was suppressed by MnTBAP in a dose-dependent manner, while during phase 2 (reoxygenation) retinal SOD activity was depleted in response to IH and MnTBAP, suggesting compromised oxidative stress defense systems in the retina during this phase despite high levels in the VF. Previous studies have shown similar high SOD levels in the vitreous of patients and loss of SOD in the vasculature with proliferative diabetic retinopathy, which correlated with increased VEGF.[32] In the present study, high vitreous SOD in response to MnTBAP, a peroxynitrite scavenger,[33] suggests accumulation. We have previously shown that the vitreous is a reservoir for growth factors[34] and therefore may reflect the ROS milieu resulting from peroxynitrite scavenging. This tight balance of antioxidant–

Table 4. Fold Change in Mitochondrial OXPHOS Genes in the Retinas of Neonatal Rats at 14 and 21 Days Postnatal Age (Data are Compared to Those for Saline-Treated 14- or 21-Day RA Littermates)

Genes of Interest	Saline O_2	MnTBAP 1 mg, RA	MnTBAP 1 mg, O_2	MnTBAP 5 mg, RA	MnTBAP 5 mg, O_2	MnTBAP 10 mg, RA	MnTBAP 10 mg, O_2
P14:							
ATPSF0E	1.1	−1.2	−457.0	1.3	−1.7	−89.4	−115.9
Cox4i1	1.3	1.1	−83.5	2.3	−1.4	1.1	−11.2
Cox8c	−1.1	1.2	−15.5	−1.0	−1.4	−1.6	−2.7
Ndufab1	−1.1	−1.0	−6.2	2.1	−1.8	−1.1	−2.7
Ndufb9	1.4	1.2	1.3	2.6	1.1	1.1	1.4
Ndufc2	1.3	1.3	1.1	2.8	−1.1	1.1	1.2
Uqcrb	22.7	23.8	21.9	53.2	16.9	22.0	22.7
P21:							
ATPSF0E	−17.5	5.7	8.9	2.5	1.4	−28.2	6.4
Cox4i1	−26.5	3.0	5.2	1.3	−3.4	2.6	2.9
Cox8a	−5.5	2.4	3.4	1.1	1.8	1.6	1.7
Ndufab1	−31.4	1.2	1.7	−1.6	−2.0	1.3	1.3
Ndufb9	1.8	2.0	1.9	1.6	2.1	1.7	−42.3
Ndufc2	63.0	84.0	77.3	74.2	67.3	80.2	67.3
Uqcrb	2.0	2.5	2.1	2.1	2.5	2.3	1.9

All data were corrected using five different housekeeping genes. Genes were selected from a focused panel of 84 genes in the OXPHOS signaling pathway. In alphabetical order, the genes of interest are *ATPSF0E* (ATP synthase H^+ transporting mitochondrial F0 complex subunit E); *Cox4i1* (cytochrome c oxidase subunit IV isoform 1); *Cox8a* (cytochrome c oxidase subunit VIIIa); *Ndufab1* (NADH dehydrogenase [ubiquinone] 1, alpha/beta subcomplex, 1); *Ndufb9* (NADH dehydrogenase [ubiquinone] 1 beta subcomplex, 9); *Ndufc2* (NADH dehydrogenase [ubiquinone] 1, subcomplex 2); *Uqcrb* (ubiquinol-cytochrome c reductase binding protein).

Investigative Ophthalmology & Visual Science

ROS systems must remain in the forefront as antioxidant therapies for ROP are explored.

The role of VEGF in oxidative stress and OIR is well documented. However, it is not known how ocular VEGF responds to exogenous antioxidants in the IH setting. Here, we show that MnTBAP treatment increased VEGF in the retina and, to a lesser degree, in the vitreous during IH. The reason for this is not clear; however, studies by Oshikawa et al.[22] demonstrate that accumulation of H_2O_2 with the use of SOD alone increases angiogenesis via VEGF/VEGFR-2 induction. Despite the trend for decreased angiogenesis with the lower doses of MnTBAP, the pathological findings of nerve fiber edema, outer nuclear layer hemorrhage, and defects in the neural retina, particularly during reoxygenation/recovery (Fig. 7), may have resulted from H_2O_2 accumulation, even with the lower doses. Studies in children with ROP showed that the photoreceptors are the primary site of retinal dysfunction.[35–37] This is confirmed in the rat model of ROP,[38,39] and suggests that hyperoxia causes damage not only to the peripheral vessels, but in the photoreceptors, and that this photoreceptor damage may even persist after the damage to the vessels has resolved.[35] It should also be noted that unlike retinal vessels, choroidal vessels, which provide oxygen to the photoreceptors, are incapable of autoregulation when tissue oxygen levels are increased, thus leading to high oxygen levels in the outer retina and accumulation of ROS and cell death. Indeed, studies by Yu et al.[40] demonstrate a relationship between H_2O_2 and autophagy. Other studies show co-occurrence of autophagy and apoptosis in photoreceptor degeneration in response to H_2O_2.[41] Soluble VEGFR-1 is a splice variant of the membrane type, VEGFR-1. It inhibits VEGF action in humans and mice by competitively binding to VEGF receptor.[42] Studies by Aiello et al.[43] showed that intravitreous injection of soluble VEGF–like chimeric proteins reduced retinal neovascularization by 50% in an animal model of ischemic retinopathy. Work by Rota et al.[44] showed an even greater decrease in retinal neovascularization in oxygen-exposed rats injected with sVEGFR-1. Our data show that endogenous sVEGFR-1 is increased in response to high VEGF levels, but this effect is abrogated with the highest dose of MnTBAP in the retina but not the VF.

The retina is a highly metabolically active tissue; therefore modifications in the retinal environment would impact the efficiency of OXPHOS. In OXPHOS, complex I (reduced nicotinamide adenine dinucleotide [NADH] dehydrogenase) is the main entrance point of electrons to the respiratory chain.[45] Complex II, or succinate dehydrogenase, is an alternate entrance point that transfers electrons from succinate to ubiquinone. Complex III, or cytochrome c reductase, is the central point in OXPHOS; complex IV or cytochrome c oxidase is the terminal complex that uses adenosine triphosphate (ATP) synthase or complex V to translocate protons across the inner mitochondrial membrane.[45] Our data showed that IH mainly affects complexes I, III, IV, and V. Phase 1 or vaso-obliteration was highly associated with upregulation of *Uqcrb* component of complex III. Previous reports suggest that the primary site for ROS generation is at complex III triggering hypoxia-inducible factor (HIF)-1α.[46] Therefore, complex III appears to be a critical point of cellular hypoxia signaling.[47–49] Inhibition of Uqcrb with terpestacin[50] or HDNT[51] inhibited hypoxia-induced angiogenesis as well as mitochondrial ROS production in tumor cells. The early activation of this gene highlights that the process of neovascularization is triggered long before phase 2 (vasoproliferation) of ROP begins according to the classical definition of ROP. However, in the "new ROP," the two phases are no longer clearly defined, with infants experiencing this variation on a minute-to-minute basis. Treatment with MnTBAP during vaso-obliteration suppressed *Cox* (complex IV) and *ATPSF0E* (complex V). This is most likely due to upregulation of uncoupling proteins, which, when under oxidative stress, are upregulated to dissociate the electron transport chain from ATP production converting the energy to heat loss and limiting further endogenous ROS production.[52] In our model of brief IH, reoxygenation at P21 was associated with upregulation of ubiquinone (complex I). Complex I is a major site of ROS production. One possible explanation for increased complex I activity is accumulation of H_2O_2.

In summary, we have shown that administration of an exogenous SOD mimetic without efficiently scavenging H_2O_2 causes photoreceptor damage and neovascularization. Furthermore, we have shown that retinal mitochondrial energy balance is disturbed in this model and that the developing retina is unable to recover. With the renewed interest in antioxidants in the preterm infant, we recommend there be an abundance of caution when pursuing these therapies, as the complex roles of antioxidants and ROS in retinal development are clearly not yet understood.

Acknowledgments

The authors thank Mark Alu, BA, of New York University Experimental Pathology Histology Core Laboratory for his technical support and assistance.

Supported by Eunice Kennedy Shriver National Institute of Child Health and Human Development Grant U54HD071594 and Memorial Medical Center Foundation, Long Beach, California, United States.

Disclosure: **S. Jivabhai Patel**, None; **F. Bany-Mohammed**, None; **L. McNally**, None; **G.B. Valencia**, None; **D.R. Lazzaro**, None; **J.V. Aranda**, None; **K.D. Beharry**, None

References

1. Gilbert C, Fielder A, Gordillo L, et al. Characteristics of infants with severe retinopathy of prematurity in countries with low, moderate, and high levels of development: implications for screening programs. *Pediatrics*. 2005;115:e518–e525.
2. Chow LC, Wright KW, Sola A, et al. Can changes in clinical practice decrease the incidence of severe retinopathy of prematurity in very low birth weight infants? *Pediatrics*. 2003; 111:339–345.
3. Smith L. Pathogenesis of retinopathy of prematurity. *Growth Hormone IGF Res*. 2004;14:S140–S144.
4. Cringle SJ, Yu DY. Oxygen supply and consumption in the retina: implications for studies of retinopathy of prematurity. *Doc Ophthalmol*. 2010;120:99–109.
5. Asikainen TM, Heikkilä P, Kaarteenaho-Wiik R, Kinnula VL, Raivio KO. Cell-specific expression of manganese superoxide dismutase protein in the lungs of patients with respiratory distress syndrome, chronic lung disease, or persistent pulmonary hypertension. *Pediatr Pulmonol*. 2001;32:193–200.
6. Saito Y, Geisen P, Uppal A, Hartnett ME. Inhibition of NAD(P)H oxidase reduces apoptosis and avascular retina in an animal model of retinopathy of prematurity. *Mol Vis*. 2007;13:840–853.
7. York JR, Landers S, Kirby RS, Arbogast PG, Penn JS. Arterial oxygen fluctuation and retinopathy of prematurity in very-low-birth-weight infants. *J Perinatol*. 2004;24:82–87.
8. Cunningham S, Fleck BW, Elton RA, McIntosh N. Transcutaneous oxygen levels in retinopathy of prematurity. *Lancet*. 1995;346:1464–1465.
9. Penn JS, Henry MM, Tolman, BL. Exposure to alternating hypoxia and hyperoxia causes severe proliferative retinopathy in the newborn rat. *Pediatr Res*. 1994;36:724–731.

10. Penn JS, Henry MM, Wall PT, Tolman BL. The range of PaO2 variation determines the severity of oxygen-induced retinopathy in newborn rats. *Invest Ophthalmol Vis Sci*. 1995;36:2063–2070.
11. Coleman R, Beharry KD, Brock RS, Abad-Santos P, Abad-Santos M, Modanlou HD. Effects of brief clustered versus dispersed hypoxic episodes on systemic and ocular growth factors in a rat model of OIR. *Pediatr Res*. 2008;64:50–55.
12. Brock RS, Gebrekristos BH, Kuniyoshi KM, Modanlou HD, Falcao MC, Beharry KD. Biomolecular effects of JB1 (an IGF-I peptide analog) in a rat model of oxygen-induced retinopathy. *Pediatr Res*. 2011;69:35–41.
13. Urata Y, Yamaguchi M, Higashiyama Y, et al. Reactive oxygen species accelerate production of vascular endothelial growth factor by advanced glycation end products in RAW264.7 mouse macrophages. *Free Radic Biol Med*. 2002;32:688–701.
14. Penn JS, Tolman BL, Bullard LE. Effect of a water soluble vitamin E analog, Trolox C, on retinal vascular development in an animal model of retinopathy of prematurity. *Free Rad Biol Med*. 1997;6:977–984.
15. Melov S, Ravenscroft J, Malik S, et al. Extension of life-span with superoxide dismutase/catalase mimetics. *Science*. 2000;289:1567–1569.
16. Melov S, Doctrow SR, Schneider JA, et al. Lifespan extension and rescue of spongiform encephalopathy in superoxide dismutase 2 nullizygous mice treated with superoxide dismutase–catalase mimetics. *J Neurosci*. 2001;21:8348–8353.
17. Beharry KD, Cai CL, Sharma P, et al. Hydrogen peroxide accumulation in the choroid during intermittent hypoxia increases risk of severe oxygen-induced retinopathy in neonatal rats. *Invest Ophthalmol Vis Sci*. 2013;54:7644–7657.
18. Higgins RD, Yu K, Sanders RJ, Nandgaonkar BN, Rotschild T, Rifkin DB. Diltiazem reduces retinal neovascularization in a mouse model of oxygen induced retinopathy. *Curr Eye Res*. 1999;18:20–27.
19. Martin RJ, Di Fiore JM, Macfarlane PM, Wilson CG. Physiologic basis for intermittent hypoxic episodes in preterm infants. *Adv Exp Med Biol*. 2012;758:351–358.
20. Di Fiore JM, Kaffashi F, Loparo K, et al. The relationship between patterns of intermittent hypoxia and retinopathy of prematurity in preterm infants. *Pediatr Res*. 2012;72:606–612.
21. Usui S, Oveson BC, Iwase T, et al. Overexpression of SOD in retina: need for increase in H_2O_2-detoxifying enzyme in same cellular compartment. *Free Radic Biol Med*. 2011;51:1347–1354.
22. Oshikawa J, Urao N, Kim HW, et al. Extracellular SOD-derived H2O2 promotes VEGF signaling in caveolae/lipid rafts and post-ischemic angiogenesis in mice. *PLoS One*. 2010;5:e10189.
23. Rao NA, Thaete LG, Delmage JM, Sevanian A. Superoxide dismutase in ocular structures. *Invest Ophthalmol Vis Sci*. 1985;12:1778–1781.
24. Hardy P, Beauchamp M, Sennlaub F, et al. Inflammatory lipid mediators in ischemic retinopathy. *Pharmacol Rep*. 2005;57:169–190.
25. Klaeger C, de Sa L, Klaeger AJ, Carlson EJ, Good WV, Epstein CJ. An elevated level of copper zinc superoxide dismutase fails to prevent oxygen induced retinopathy in mice. *Br J Ophthalmol*. 1996;80:429–434.
26. Andreyev AY, Kushnareva YE, Starkov AA. Mitochondrial metabolism of reactive oxygen species. *Biochemistry (Moscow)*. 2005;70:200–214.
27. Lee JW, Davis JM. Future applications of antioxidants in premature infants. *Curr Opin Pediatr*. 2011;22:161–166.
28. Awad JA, Roberts LJ, Burk RF, Morrow JD. Isoprostanes–prostaglandin-like compounds formed in vivo independently of cyclooxygenase. *Gastroenterol Clin North Am*. 1996;25:409–427.
29. Roberts LJ, Morrow JD. The generation and actions of isoprostanes. *Biochem Biophys Acta*. 1997;1345:121–135.
30. Gu X, El-Remessy AB, Brooks SE, Al-Shabrawey M, Tsai N-T, Caldwell RB. Hyperoxia induces retinal vascular endothelial cell apoptosis through formation of peroxynitrite. *Am J Physiol Cell Physiol*. 2003;285:C546–C554.
31. Neisman MR, Johnson KA, Penn JS. Therapeutic effect of liposomal superoxide dismutase in an animal model of ROP. *Neurochem Res*. 1997;22:597–605.
32. Izuta H, Chikaraishi Y, Adachi T, et al. Extracellular SOD and VEGF are increased in vitreous bodies from vasoproliferative diabetic retinopathy patients. *Mol Vis*. 2009;15:2663–2672.
33. Batinic-Haberle I, Cuzzocrea S, Reboucas JS, et al. Pure MnTBAP selectively scavenges peroxynitrite over superoxide: comparison of pure and commercial MnTBAP samples to MnTE-2-PyP in two different models of oxidative stress injuries, SOD-specific E. coli model and carrageenan-induced pleurisy. *Free Radic Biol Med*. 2009;46:192–201.
34. Modanlou HD, Gharraee Z, Hasan J, Waltzman J, Nageotte S, Beharry KD. Ontogeny of VEGF, IGF-I, and GH in neonatal rat serum, vitreous fluid, and retina from birth to weaning. *Invest Ophthalmol Vis Sci*. 2006;47:738–744.
35. Fulton AB, Hansen RM. Photoreceptor function in infants and children with a history of mild retinopathy of prematurity. *J Opt Soc Am A Opt Image Sci Vis*. 1996;13:566–571.
36. Fulton AB, Hansen RM, Petersen RA, Vanderveen DK. The rod photoreceptors in retinopathy of prematurity: an electroretinographic study. *Arch Ophthalmol*. 2001;119:499–505.
37. Fulton AB, Hansen RM, Moskowitz A, Akula JD. The neurovascular retina in retinopathy of prematurity. *Prog Retin Eye Res*. 2009;28:452–482.
38. Liu K, Akula JD, Hansen RM, Moskowitz A, Kleinman MS, Fulton AB. Development of the electroretinographic oscillatory potentials in normal and ROP rats. *Invest Ophthalmol Vis Sci*. 2006;47:5447–5452.
39. Dembinska O, Rojas LM, Varma DR, Chemtob S, Lachapelle P. Graded contribution of retinal maturation to the development of oxygen-induced retinopathy in rats. *Invest Ophthalmol Vis Sci*. 2001;42:1111–1118.
40. Yu L, Wan F, Dutta S, et al. Autophagic programmed cell death by selective catalase degradation. *Proc Natl Acad Sci U S A*. 2006;103:4952–4957.
41. Kunchithapautham K, Rohrer B. Apoptosis and autophagy in photoreceptors exposed to oxidative stress. *Autophagy*. 2007;3:433–441.
42. Roy H, Bhardwaj S, Yla-Herttuala S. Biology of vascular endothelial growth factors. *FEBS Lett*. 2006;580:2879–2887.
43. Aiello LP, Pierce EA, Foley ED, et al. Suppression of retinal neovascularization in vivo by inhibition of vascular endothelial growth factor (VEGF) using soluble VEGF-receptor chimeric proteins. *Proc Natl Acad Sci U S A*. 1995;92:10457–10461.
44. Rota R, Riccini T, Zaccarini M, et al. Marked inhibition of retinal neovascularization in rats following soluble-flt-1 gene transfer. *J Gene Med*. 2004;6:992–1002.
45. Dudkina NV, Sunderhaus S, Boekema EJ, Braun H-P. The higher level of organization of the oxidative phosphorylation system: mitochondrial supercomplexes. *J Bioenerg Biomembr*. 2008;40:419–424.
46. Guzy R, Schumaker P. Oxygen sensing by mitochondria at complex III: the paradox of increased ROS during hypoxia. *Exp Physiol*. 2006;5:807–819.
47. Guzy RD, Hoyos B, Robin E, et al. Mitochondrial complex III is required for hypoxia-induced ROS production and cellular oxygen sensing. *Cell Metab*. 2005;1:401–408.
48. Chandel NS, Maltepe E, Goldwasser E, et al. Mitochondrial reactive oxygen species trigger hypoxia-induced transcription. *Proc Natl Acad Sci U S A*. 1998;95:11715–11720.

Investigative Ophthalmology & Visual Science

49. Brunelle JK, Bell EL, Quesada NM, et al. Oxygen sensing requires mitochondrial ROS but not oxidative phosphorylation. *Cell Metab*. 2005;1:409–414.
50. Jung HJ, Shim JS, Lee J, et al. Terpestacin inhibits tumor angiogenesis by targeting UQCRB of mitochondrial complex III and suppressing hypoxia-induced reactive oxygen species production and cellular oxygen sensing. *J Biol Chem*. 2010; 285:11584–11595.
51. Jung HJ, Kim KH, Kim ND, Han G, Kwon HJ. Identification of a novel small molecule targeting UQCRB of mitochondrial complex III and its anti-angiogenic activity. *Bioorg Med Chem Lett*. 2011;21:1052–1056.
52. Cui Y, Xu X, Bi H, et al. Expression modification of uncoupling proteins and MnSOD in retinal endothelial cells and pericytes induced by high glucose: the role of ROS in diabetic retinopathy. *Exp Eye Res*. 2006;83:807–816.

Investigative Ophthalmology & Visual Science